

P4.2 LABORATORY AND NUMERICAL STUDIES OF VERY STABLE BOUNDARY LAYERS

Yuji Ohya* and Takanori Uchida

Research Institute for Applied Mechanics, Kyushu University, Japan

1. INTRODUCTION

The turbulence structure and transport process of SBL with a wide variety of stability have not yet been fully clarified, because of the difficulties of measurement and the complexity associated with unsteadiness and non-uniformity of SBL (Stull, 1988 ; Mahrt, 1999). Recently, Mahrt (1999) has discussed various features of different stability regimes of SBL, focusing on the very stable case, and pointed out that similarity theory and the traditional concept of a boundary layer break down for the very stable case.

For the laboratory studies of SBL in the past, the stably stratified flows obtained have been limited within relatively weak stabilities. Moreover, it is difficult to simulate SBLs with various different vertical profiles of mean temperature because of the limited capability of wind tunnels. In the previous studies (Ohya, et al., 1997 ; Ohya, 2001), we have simulated a common type of SBL, in which the mean temperature increases upward in an exponential or polynomial manner. We have investigated the turbulence structure and transport process, and have obtained a number of interesting features, leading to a better understanding of SBL. For the present study, we have developed a simulation method for another type of SBL, in which the mean temperature increases upward linearly, by using a specially designed thermally stratified wind tunnel. In parallel with wind tunnel experiments, to understand the turbulence features and fluid dynamics in detail, we have also performed numerical simulations of the SBL. From both the wind tunnel experiment and numerical simulation, we have investigated the flow structure and turbulence transport process of SBL with a wide range of stability, noting the influence of the different vertical profiles of mean temperature on the turbulence phenomena.

2. THERMALLY STRATIFIED WIND TUNNEL AND EXPERIMENTAL METHOD

Experiments were performed in a thermally stratified wind tunnel of Kyushu University (Ohya, et al., 1996). The experimental arrangement for the present SBL simulations is shown in Figure 1. SBL flows that show a linear increase in the mean-temperature profile is created by heating the wind

tunnel airflow and by cooling the test-section floor at around 9 °C . A preshaping vertical profile of temperature is set with the air-flow heating unit which is placed the upstream of the test section. The stratified turbulent boundary layer with freestream velocities, $U_\infty = 0.7 - 1.9 \text{ ms}^{-1}$, covers a range of stability from neutral to strongly stable. As summarized in Table 1, the Reynolds number, $Re_\delta = (U_\infty \delta / \nu)$, based on the boundary layer thickness, δ , ranges (2.9 - 5.3) $\times 10^4$. The bulk Richardson number, $Ri_\delta = (g/\theta_o) \cdot (\theta_\infty - \theta_s) \delta / U_\infty^2$, ranges from 0 to 1.38. Here, ν is the coefficient of kinematic viscosity, g , the acceleration due to gravity, θ_o , the average absolute temperature over the whole boundary layer depth, θ_s , the temperature of cooled floor, θ_∞ , the temperature of ambient air at δ . Measurements of turbulent quantities in the vertical direction were made at a distance of 9 m downstream from the 2D fence where the boundary layer is fully developed. The simultaneously using a sensor system of an X-type hot-wire and an I-type cold-wire. Flow visualization of the simulated SBL was also carried out with a smoke-wire device placed inside the test section.

3. NUMERICAL METHOD

Direct numerical simulations of stratified boundary layers under various stability conditions were also made by a finite-difference method without any turbulence model. The calculation domain is 9m long (x-direction), 1m wide (y-direction), 1m high (z-direction). A Cartesian grid system consists of uniform horizontal grids and vertical non-uniform grids concentrated toward the ground. The number of grid points in the x, y and z directions is 601x101x91. Under the Boussinesq approximation, the governing equations consist of the Navier-Stokes, continuity and energy equations for 3D incompressible stratified flow. The boundary conditions are almost similar to those in the wind tunnel experiments except for the surface roughness by chain over the test section floor. The numerical method is a variant of a fractional-step method. For time advance, the Euler explicit method is used. All the spatial derivatives are approximated with second-order central differences on a staggered grid. The computational data of neutral and stratified flows are shown in Table 2.

4. RESULTS

4.1 Vertical profiles of turbulent quantities

The vertical profiles in Figures 2-4 are normalized

*Corresponding author address : Yuji Ohya, Research Institute for Applied Mechanics, Kyushu University, 6-1 Kasuga-koen, Kasuga 816-8580, Japan ; e-mail : ohya@riam.kyushu-u.ac.jp

by the ambient velocity U_∞ and temperature difference $\Delta\theta (= \theta_\infty - \theta_s)$, and are shown with the normalized height z/δ . Figures 2a-c show the vertical profiles of mean U -velocity and temperature θ . As seen in Figures 2b, c, the mean temperature θ almost linearly increases upward for all stable cases in both experimental and numerical simulations.

Figures 3a-d show the vertical profiles of normalized fluctuation intensities (σ means the r.m.s. value) of u -velocity component and temperature θ , both from experiment and calculation. The linear stable stratification strongly suppresses the fluctuations of velocity and temperature. Similar to the other type of SBL (Ohya, 2001), these profiles display great differences in the lower half of the boundary layer. For the weak stability cases S1 and S2, the u -velocity fluctuations are decreased with increasing stability. As seen in Figures 3c, d, it should be noted that the vertical profile of temperature fluctuation intensity for the very weak stability case S1 is remarkably different from those for other type of SBLs (Ohya, 2001). A maximum of temperature fluctuation appears in the middle height range of boundary layer. This is caused by the interaction between the upward bursting of turbulence and the large temperature gradient in the upper height, similar to the maximum of the temperature fluctuation in the capping inversion layer for convective boundary layers (CBL). It is reported that the vertical profiles of temperature variance are greatly different among the observational results (Nieuwstadt, 1984). The present experiment suggests that it is mainly caused by the difference in vertical mean-temperature profiles. On the other hand, for strong stability case S3, the u -velocity fluctuation decreases to zero as z/δ approach zero, as seen in Figures 3a, b. In particular, it should be noted that a maximum of velocity fluctuation clearly appears in the lower part of the boundary layer, say at around $z/\delta = 0.3$.

As shown in Figures 4a-d, momentum and heat fluxes are also significantly decreased with increasing stability for weak stability cases S1 and S2. For strong stability case S3, momentum and heat fluxes become nearly zero over the whole boundary layer depth.

Similar to the other type of SBL (Ohya, 2001), the vertical profiles of turbulence quantities exhibit different behavior in two distinct stability regimes of the SBL flows with weak stability and those with strong stability, as shown in Figures 2-4. To investigate the reason, we have displayed the vertical profiles of time-mean local gradient Richardson number Ri for each SBL flow case in Figure 5. The straight broken line at a value of $Ri = 0.25$ in Figure 5 shows the critical Richardson number Ri_{cr} given by a linearized theory for inviscid flow. We should note that the two groups of SBL flows with weak and strong stability correspond to the two groups of the Ri profiles, separated by the Ri_{cr} . Namely, in the lower part of boundary layer, say $z/\delta < 0.3$, the Ri profiles with the weak stability group are smaller than Ri_{cr} , whereas the Ri profiles with the strong stability group are larger than Ri_{cr} .

4.2 Flow visualization

Figure 6 shows the results of flow visualization experiment by the smoke-wire method. For the weak stability case S1, as seen in Figure 6a, the flow pattern is similar to that for a neutral turbulent boundary layer. We can see a vigorous mixing in the lower part of the boundary layer. On the other hand, as seen in Figure 6b, wave-like motions due to Kelvin-Helmholtz (K-H) instability and the rolling up and breaking of the K-H waves can be observed very frequently in the lower part of boundary layer for a SBL flow with strong stability (case S3). We speculate that in very stable boundary layers, wind shear can increase locally because of the lack of mixing. Eventually, the shear is strong enough to trigger shear instability and turbulence (i.e., the local Richardson number is lower enough than Ri_{cr}). This shear instability corresponds to breaking K-H wave. The resulting turbulence mixes both heat and momentum, causing the shear to decrease and the Richardson number to increase. Eventually, the shear is too weak to support shear instability and turbulence, and both cease. During the resulting quiescent period, shear can again build to the point of shear instability or turbulence. Such a scenario can occur repeatedly (Stull, 1988 ; Coulter, 1990 ; Mahrt, 1999). Thus, for the lower part of a boundary layer with strong stability, turbulence and waves clearly coexist. The K-H instability occurs very frequently and the development and breaking of the K-H waves are repeated. This event leads to distinct fluctuations of velocity and temperature decoupled from the surface, corresponding to the maximum of velocity fluctuations at around $z/\delta = 0.3$, as shown in Figures 3a, b. Figures 7a-c show the time histories of w , θ and $w\theta$ at $z/\delta = 0.29$ for case S3. As shown in Figure 7c, the instantaneous transfer of turbulent fluxes frequently occurs in the both gradient and counter-gradient directions, although the time-mean transfer of turbulent fluxes is almost zero.

Moreover, wavy motions with a long wavelength (approximately 1-2 m) driven by buoyancy can also be observed in the upper part of all stable boundary layers (cases S1-S3). The cross spectrum analysis of w and θ suggests that the fluctuations of w and θ are strongly influenced by a wavy motion with a long wavelength, such as an internal gravity wave.

5. CONCLUSIONS

We have successfully simulated a type of stable boundary layers (SBL), in which the mean temperature increases upward almost linearly, by using a thermally stratified wind tunnel. The effects of strong stable stratification on the turbulence boundary layer are investigated. The main results obtained are as follows. 1) The vertical profiles of turbulence quantities exhibit different behavior in two distinct stability regimes of the SBL flows with weak and strong stability, corresponding to the difference in the vertical profiles of the local Richardson number Ri , which are separated by the critical Richardson number Ri_{cr} .

2) For strong stability cases, wavy motions due to Kelvin-Helmholtz shear instability and the rolling up and breaking of those waves can be observed very frequently in the lower part of boundary layer. The wavy motions and turbulence due to wave breaking lead to a maximum of the velocity fluctuation decoupled from the surface.

3) For the upper part of all stable boundary layers, the flows are almost nonturbulent and still have large temperature gradients. The appearance of internal gravity waves is suggested from cross-spectrum analyses.

4) For weak stability cases, the transfer of turbulent momentum and heat fluxes is basically similar to those for the neutral turbulent boundary layers, although they are weakened with increasing stability.

5) On the other hand, for strong stability cases, the time-mean transfer of turbulent fluxes is almost zero for the whole boundary layer depth. However, the instantaneous transfer of turbulent fluxes frequently occurs in the both gradient and counter-gradient directions in the lower part of boundary layer. This is due to the Kelvin-Helmholtz (K-H) instability and the rolling up and breaking of K-H waves.

References

- Coulter, R. L. : 1990, 'A Case Study of Turbulence in the Stable Nocturnal Boundary Layer', *Boundary-Layer Meteor.* **52**, 75-91.
- Mahrt, L. : 1999, 'Stratified Atmospheric Boundary Layers', *Bound.-Layer Meteor.*, **90**, 375-396.
- Nieuwstadt, F. T. M. : 1984a, 'The Turbulent Structure of the Stable, Nocturnal Boundary Layer', *J. Atmos. Sci.* **41**, 2202-2216.
- Ohya, Y., Neff, D. E. and Meroney, R. N. : 1997, 'Turbulence structure in a stratified boundary layer under stable conditions', *Bound.-Layer Meteor.*, **83**, 139-161.
- Ohya, Y. : 2001, 'Wind tunnel study of atmospheric stable boundary layers over a rough surface', *Bound.-Layer Meteor.*, **98**, 57-82.
- Ohya, Y., Tatsuno, M., Nakamura, Y., and Ueda, H. : 1996, 'A thermally stratified wind tunnel for environmental flow studies', *Atmos. Environ.*, **30**, 2881-2887.
- Stull, R. B. : 1988, *An Introduction to Boundary Layer Meteorology*, Kluwer Academic Publishers, pp. 499-502 and 513 (666 pp.).

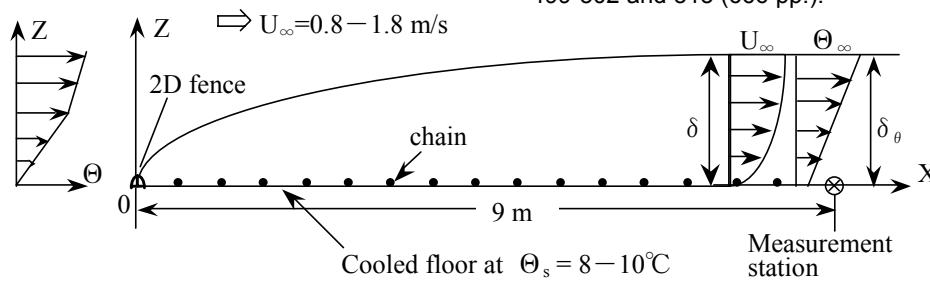


Figure 1. Experimental arrangement.

Exp. case	N1	S1	S2	S3
U_∞ (ms ⁻¹)	1.76	1.57	1.11	0.86
Re_δ	52800	43500	30700	29300
Ri_δ	—	0.28	0.56	1.38
δ (m)	0.45	0.45	0.45	0.55
$\Delta \Theta$ (°C)	—	47.4	47.0	57.9
u_* / U_∞	0.054	0.032	0.028	—
L (m)	∞	0.34	0.12	—
Symbol	●	□	△	○

Table 1. Experimental conditions for neutral (case N1) and stable boundary layers (cases S1-S3).

Cal. case	N1	S1	S2	S3
U_∞ (ms ⁻¹)	1.08	1.09	1.1	1.12
Re_δ	5400	5450	5500	6720
Ri_δ	—	0.17	0.85	1.69
δ (m)	0.5	0.5	0.5	0.6
$\Delta \Theta$ (°C)	—	66	65.3	70.5
u_* / U_∞	0.051	0.04	0.029	0.025
Symbol	●	□	△	○

Table 2. Numerical conditions for neutral (case N1) and stable boundary layers (cases S1-S3).

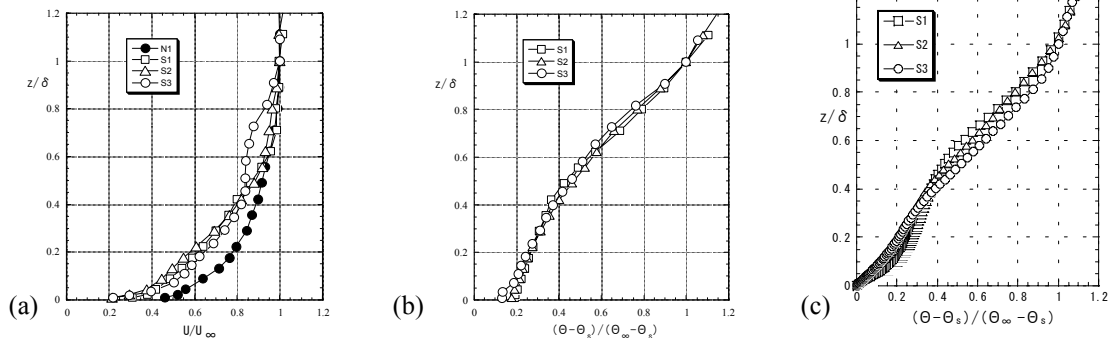


Figure 2. Vertical profiles of the mean velocity and temperature: (a) Streamwise velocity U , (b, c) temperature Θ

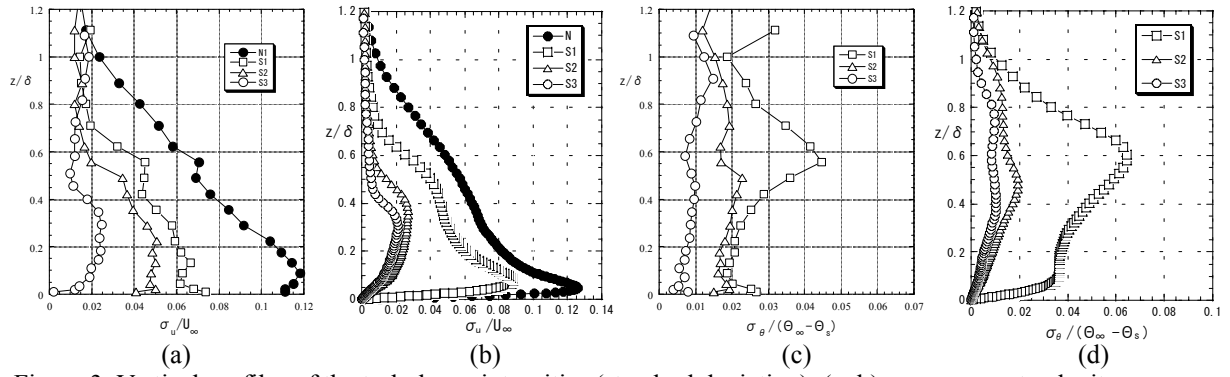


Figure 3. Vertical profiles of the turbulence intensities (standard deviation): (a, b) u -component velocity σ_u , (c, d) temperature σ_θ . (a, c) : Experiment, (b, d) : Calculation

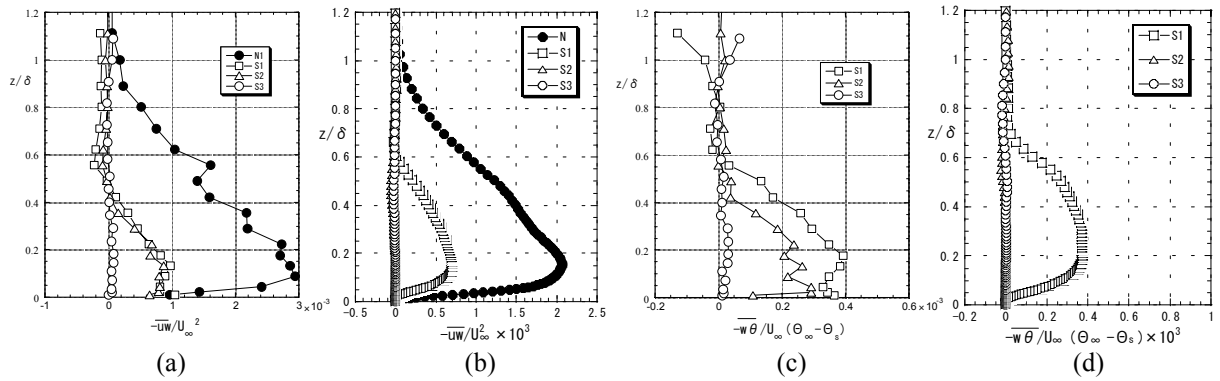


Figure 4. Vertical profiles of the turbulence fluxes: (a, b) Momentum flux $-uw$, (c, d) vertical heat flux $-w\theta$. (a, c) : Experiment, (b, d) : Calculation

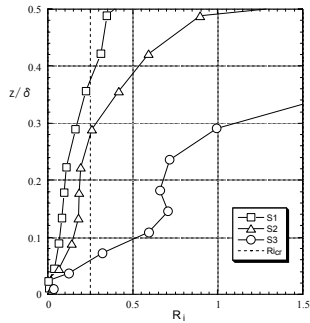


Figure 5. Vertical profiles of the local gradient Richardson number Ri .

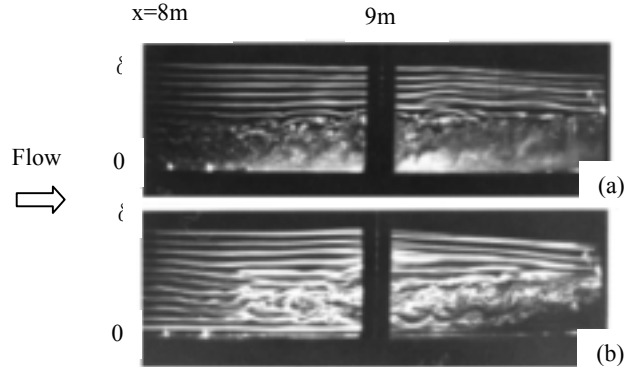


Figure 6. Flow visualization of stable boundary layers : (a) case S1, (b) case S3.

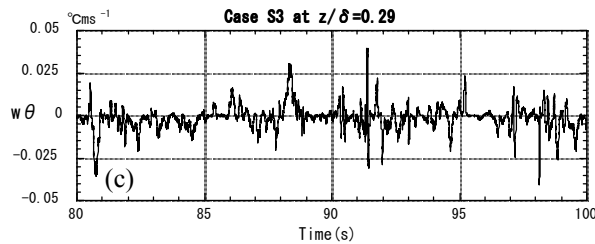
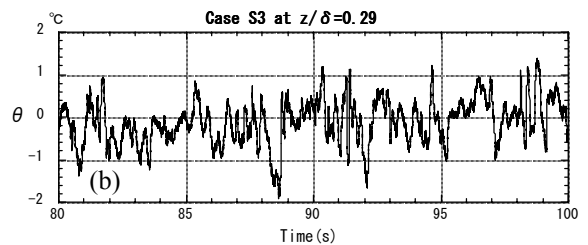
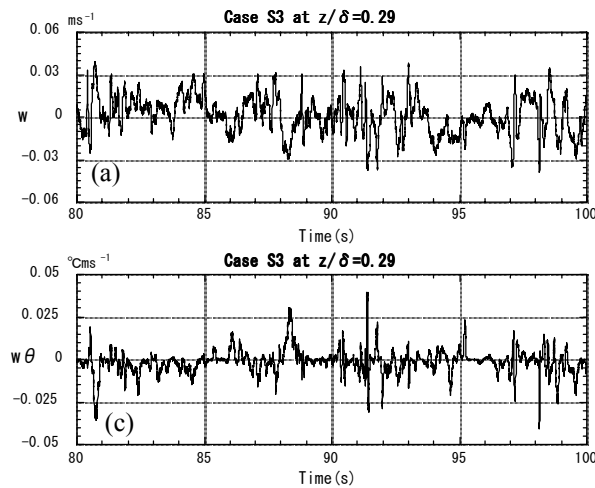


Figure 7. Time histories of w , θ and $w\theta$ fluctuations for case S3 at $z/\delta=0.29$: (a) w fluctuation, (b) θ fluctuation, (c) $w\theta$ fluctuation.